

Coherent hole burning and Mollow absorption effects in the cycling transition $F_e=0 \leftrightarrow F_g=1$ subject to a magnetic field

Ying Gu,^{*} Qingqing Sun, and Qihuang Gong[†]*State Key Laboratory for Mesoscopic Physics, Department of Physics, Peking University, Beijing 100871, China*

(Received 4 January 2004; published 7 June 2004)

With saturation and probing by circularly polarized fields, quantum coherence effects are investigated for the cycling transition $F_e=0 \leftrightarrow F_g=1$, which is subject to a linearly polarized field and a magnetic field. The saturation field is applied to the case of maximum coherence between the drive Rabi frequency and magnetic field, corresponding to the electromagnetically induced absorption (EIA) with negative dispersion found by Gu *et al.* For a small saturation Rabi frequency, holes are burned in two Autler-Towns peaks outside two symmetric electromagnetically induced transparency windows due to the two-photon resonance. However, when the saturation Rabi frequency is comparable with the drive Rabi frequency, holes caused by the coherent population oscillation appear in the EIA spectrum. Finally, when the saturation Rabi frequency is large enough, several emission peaks are observed due to the Mollow absorption effects. Furthermore, the dispersion at the pump-probe detuning center is kept negative with an increase in saturation field, which is a precursor of superluminal light propagation.

DOI: 10.1103/PhysRevA.69.063805

PACS number(s): 42.50.Gy, 32.80.Qk, 42.25.Kb

I. INTRODUCTION

Recently, quantum coherence effects in degenerate atomic systems have attracted great interest. On the one hand, they possess the general features of the Λ - and V-type systems, such as electromagnetically induced transparency (EIT) [1], coherent population trapping (CPT) [2], and the enhanced refractive index effect [3]. On the other hand, the degeneracy of atomic energy influences the refraction and absorption in the phase-coherent atomic ensemble. EIT and electromagnetically induced absorption (EIA) have been predicted and observed in the degenerate systems due to the atomic coherence among Zeeman sublevels belonging to the same hyperfine splitting [4–7]. Absorption spectra of the degenerate two-level atomic system driven by optical fields are different from the classical Mollow absorption spectrum (MAS) [8–10]. With the Zeeman splitting, the two-level degenerate atomic system also shares the properties of the multilevel atom. In this paper, we investigate the quantum coherence effects of a degenerate atomic system for the transition $F_e=0 \leftrightarrow F_g=1$ driven by a linearly polarized field and saturated by the circularly polarized fields.

Hole burning in homogenous and inhomogeneous Doppler-broadened atoms was studied since the 1960s [11–14]. The saturation spectra can be used to study the collision process in atomic and molecular systems [15], as well as the writing and reading of optical data [16,17]. Recently, hole burning and anti-hole-burning caused by the coherent population oscillations are used to demonstrate the subluminal and superluminal light propagation in solids [18,19]. In the degenerate two-level atomic system for a transition $F_e=0 \leftrightarrow F_g=1$, when the coherence between the drive Rabi frequency and Zeeman splitting reaches the maximum, the EIA

with negative dispersion is reported [20]. Also for this transition, in this work, the saturation fields are added (detailed description in Sec. II). We find coherent hole burning and Mollow absorption in the original EIA spectra [20] with varying the saturation field.

In the following, we will investigate the quantum coherence effects for the cycling transition $F_e=0 \leftrightarrow F_g=1$ driven by a linearly polarized field, saturated and probed by the circular polarized field, and in a magnetic field. Without the saturation field, when the drive Rabi frequency equals the Zeeman splitting, the quantum coherence reaches the maximum, namely, EIA with negative dispersion has been obtained due to the shifting of EIT windows [20]. Then, for the fixed drive Rabi frequency where EIA occurs, the saturation field is added. In a small saturation Rabi frequency, the holes are burned in the Autler-Towns peaks outside the two symmetric EIT windows due to the two-photon resonance [21]. When the saturation Rabi frequency is matching with the drive Rabi frequency, the holes caused by the coherent population oscillation [22,23] appear in the original EIA spectrum [20]. When we continue to increase the saturation field, several emission peaks are observed due to the Mollow absorption effects [9,10]. With the increment of the saturation field, the dispersion at the pump-probe detuning center is kept to be negative, which predicts the superluminal light propagation. Finally, the situations beyond the EIA are discussed. When the drive Rabi frequency is very small, first four EIT windows, then Mollow absorption appears in the absorption spectrum with increasing the saturation Rabi frequency. However, when the drive Rabi frequency is very large, the intensive saturation field only leads to the widening of the EIT window at the zero pump-probe detuning.

The paper is organized as follows. In the next section, we set up the theoretical model for the transition $F_e=0 \leftrightarrow F_g=1$ in the drive, saturation and probe fields, and write out its optical Bloch equations. Considering various photonic processes of the transitions, we express the Bloch equations as a

^{*}Email address: ygu@pku.edu.cn

[†]Email address: qhgong@pku.edu.cn

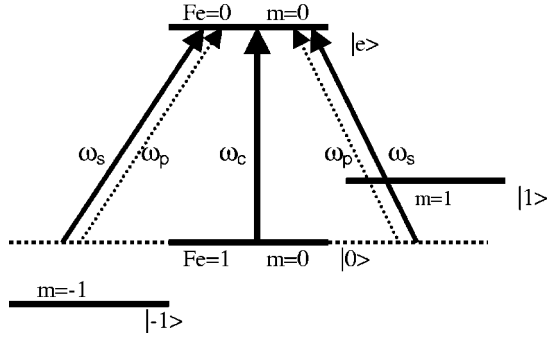


FIG. 1. Diagram of the energy levels for a cycling transition $F_e=0 \leftrightarrow F_g=1$. It is driven by a linearly polarized π field with frequency ω_c , saturated and probed by the circularly polarized fields σ_{\pm} with ω_s and ω_p .

set of linear equations of Fourier amplitudes. Then, in Sec. III, we solve these linear equations numerically and discuss the quantum coherence effects with varying the drive Rabi frequency and saturation Rabi frequency. Finally, a summary is given in Sec. IV.

II. THEORETICAL APPROACH

The simplest degenerate two-level system is considered. As shown in Fig. 1, a degenerate two-level transition $F_e=0 \leftrightarrow F_g=1$ is set up, which is used to represent a set of transitions $F_e \leftrightarrow F_g = F_e + 1$. The atomic system is driven by a linearly polarized π field with frequency ω_c , saturated and probed by the circularly polarized fields σ_{\pm} with frequency ω_s and ω_p . Note that the polarization of the saturation fields and probe fields is orthogonal to the linear polarization of the drive field and magnetic field. If the magnetic field is defined as the quantization axis. The saturation and probe field propagation direction and drive field polarization direction are parallel to quantization axis, while the saturation and probe field oscillations are orthogonal to the quantization axis. Here π field interacts with the transition $M_{F_e} = i \leftrightarrow M_{F_g} = i$, and σ_{\pm} field interacts with the transition $M_{F_e} = i \leftrightarrow M_{F_g} = i \pm 1$ with $i=0, \pm 1$. In the presence of magnetic field, the system is a closed four-level one. A transition $F_e=0 \leftrightarrow F_g=1$ can be experimentally realized by using the $4f^6 6s^2 {}^7F_1 \leftrightarrow 4f^6 6s 6p {}^5D_0$ transition of Sm [24,25] and the $2p^5 3s {}^3P_1 \leftrightarrow 2p^5 3p {}^3P_0$ transition of Ne* [26]. A transition $5S_{1/2}(F=1) \leftrightarrow 5P_{3/2}(F=0)$ in the D_2 line of ^{87}Rb [27] is also a good example, however, in that case, the $M_{F_g} = -1$ level is higher in energy than the $M_{F_g} = 1$ level. All transition have the same magnitude of dipole moments, but with the different sign, i.e., $\mu_{e1} = \mu_{e-1} = -\mu_{e0} = \mu$.

Now we consider only the decay of the atomic levels due to the spontaneous emission and the collisions that result in dephasing of the coherence and exchange of population between the ground state levels. In the rotating-wave approximations, the system is governed by the optical Bloch equations:

$$\begin{aligned} \dot{\rho}_{ee} = & \frac{i}{\hbar}(V_{e-1}\rho_{-1e} - \rho_{e-1}V_{-1e}) + \frac{i}{\hbar}(V_{e1}\rho_{1e} - \rho_{e1}V_{1e}) \\ & + \frac{i}{\hbar}(V_{e0}\rho_{0e} - \rho_{e0}V_{0e}) - (\Gamma_{e-1} + \Gamma_{e1} + \Gamma_{e0})\rho_{ee}, \end{aligned} \quad (1)$$

$$\begin{aligned} \dot{\rho}_{-1-1} = & -\frac{i}{\hbar}(V_{e-1}\rho_{-1e} - \rho_{e-1}V_{-1e}) - (\Gamma_{-10} + \Gamma_{-11})\rho_{-1-1} \\ & + \Gamma_{e-1}\rho_{ee} + \Gamma_{0-1}\rho_{00} + \Gamma_{1-1}\rho_{11}, \end{aligned} \quad (2)$$

$$\begin{aligned} \dot{\rho}_{11} = & -\frac{i}{\hbar}(V_{e1}\rho_{1e} - \rho_{e1}V_{1e}) - (\Gamma_{10} + \Gamma_{1-1})\rho_{11} + \Gamma_{e1}\rho_{ee} \\ & + \Gamma_{01}\rho_{00} + \Gamma_{-11}\rho_{-1-1}, \end{aligned} \quad (3)$$

$$\begin{aligned} \dot{\rho}_{00} = & -\frac{i}{\hbar}(V_{e0}\rho_{0e} - \rho_{e0}V_{0e}) - (\Gamma_{0-1} + \Gamma_{01})\rho_{00} + \Gamma_{e0}\rho_{ee} \\ & + \Gamma_{-10}\rho_{-1-1} + \Gamma_{10}\rho_{11}, \end{aligned} \quad (4)$$

$$\begin{aligned} \dot{\rho}_{e-1} = & -\frac{i}{\hbar}[V_{e-1}(\rho_{ee} - \rho_{-1-1}) - V_{e1}\rho_{1-1} - V_{e0}\rho_{0-1}] \\ & - (i\omega_{e-1} + \gamma_{e-1})\rho_{e-1}, \end{aligned} \quad (5)$$

$$\begin{aligned} \dot{\rho}_{e1} = & -\frac{i}{\hbar}[V_{e1}(\rho_{ee} - \rho_{11}) - V_{e-1}\rho_{-11} - V_{e0}\rho_{01}] \\ & - (i\omega_{e1} + \gamma_{e1})\rho_{e1}, \end{aligned} \quad (6)$$

$$\begin{aligned} \dot{\rho}_{e0} = & -\frac{i}{\hbar}[V_{e0}(\rho_{ee} - \rho_{00}) - V_{e-1}\rho_{-10} - V_{e1}\rho_{10}] \\ & - (i\omega_{e0} + \gamma_{e0})\rho_{e0}, \end{aligned} \quad (7)$$

$$\dot{\rho}_{1-1} = -\frac{i}{\hbar}(V_{e-1}\rho_{1e} - \rho_{e-1}V_{1e}) - (i\omega_{1-1} + \gamma_{1-1})\rho_{1-1}, \quad (8)$$

$$\dot{\rho}_{10} = -\frac{i}{\hbar}(V_{e0}\rho_{1e} - V_{1e}\rho_{e0}) - (i\omega_{10} + \gamma_{10})\rho_{10}, \quad (9)$$

$$\dot{\rho}_{-10} = -\frac{i}{\hbar}(V_{e0}\rho_{-1e} - V_{-1e}\rho_{e0}) - (i\omega_{-10} + \gamma_{-10})\rho_{-10}, \quad (10)$$

$$\dot{\rho}_{ij} = \dot{\rho}_{ji}^*. \quad (11)$$

Ignoring the effect of spatial amplitude, the interaction energy V_{ei} for the $|e\rangle \rightarrow |i\rangle$ transition can be expressed as $V_{e1} = V_{e-1} = \hbar V_s(\omega_s)e^{-i\omega_s t} + \hbar V_p(\omega_p)e^{-i\omega_p t}$ and $V_{e0} = \hbar V_c(\omega_c)e^{-i\omega_c t}$. Here the magnitude values of $2V_c(\omega_c) = -\mu E_c/2^{1/2}\hbar$, $2V_s(\omega_s) = \mu E_s/2^{1/2}\hbar$ and $2V_p(\omega_p) = \mu E_p/2^{1/2}\hbar$ are defined as the drive Rabi frequency, saturation Rabi frequency and probe Rabi frequency, respectively. Let $\omega_{ij} = \omega_i - \omega_j$. $\omega_{1-1} = 2g\mu_b B/\hbar$ denotes the Raman detuning induced by the static magnetic field of strength B applied in the atoms, where g is the Lande factor and μ_b the Bohr magneton. Γ_{ij} is the decay rate from state $|i\rangle$ to $|j\rangle$. Here we set $\Gamma_{e1} = \Gamma_{e-1} = \Gamma_{e0} = \Gamma$. The decay rate among three lower levels is small and the same, i.e., $\Gamma_{ij} = \Gamma_0$ for $i, j = 1, 0, -1 (i \neq j)$. Ignoring the rate of dephasing collisions, we have $\gamma_{e-1} = \gamma_{e0} = \gamma_{e1} = \gamma = (3\Gamma + 2\Gamma_0)/2$ and $\gamma_{1-1} = \gamma_{10} = \gamma_{-10} = \gamma_0 = 2\Gamma_0$.

We treat the drive field to all orders in E_c and E_s , and the probe field to the first order in E_p . In the steady state, the elements of the density matrix are expressed as the terms of Fourier amplitudes [22,28]. Each Fourier amplitude can be used to represent a photonic process. For example, the third order nonlinear term $\rho_{e0}(\omega_c + \omega_p - \omega_s)$ means a three-photon process from the state $|0\rangle$ to $|e\rangle$, where the atom in the state $|0\rangle$ absorbs a ω_c photon to $|e\rangle$, and simultaneously emits a ω_s photon to the state $|1\rangle$ or $|-1\rangle$ and absorbs a ω_p photon back to $|e\rangle$. Considering various photonic process, in terms of the Fourier amplitudes $\rho_{ei}(\omega_i)$, we express ρ_{ii} as

$$\rho_{ii} = \rho_{ii}^{dc} + \rho_{ii}(\omega_p - \omega_s)e^{-i(\omega_p - \omega_s)t} + \rho_{ii}(\omega_s - \omega_p)e^{-i(\omega_s - \omega_p)t} \quad (12)$$

with $i=e, 1, 0, -1$;

$$\begin{aligned} \rho_{e0} = & \rho_{e0}(\omega_c)e^{-i\omega_c t} + \rho_{e0}(\omega_c + \omega_p - \omega_s)e^{-i(\omega_c + \omega_p - \omega_s)t} \\ & + \rho_{e0}(\omega_c - \omega_p + \omega_s)e^{-i(\omega_c - \omega_p + \omega_s)t}, \end{aligned} \quad (13)$$

$$\rho_{ei} = \rho_{ei}(\omega_s)e^{-i\omega_s t} + \rho_{ei}(\omega_p)e^{-i\omega_p t} + \rho_{ei}(2\omega_s - \omega_p)e^{-i(2\omega_s - \omega_p)t} \quad (14)$$

with $i=1, -1$;

$$\begin{aligned} \rho_{0i} = & \rho_{0i}(\omega_p - \omega_c)e^{-i(\omega_p - \omega_c)t} + \rho_{0i}(\omega_s - \omega_c)e^{-i(\omega_s - \omega_c)t} \\ & + \rho_{0i}(2\omega_s - \omega_p - \omega_c)e^{-i(2\omega_s - \omega_p - \omega_c)t} \end{aligned} \quad (15)$$

with $i=1, -1$; and ρ_{-11} reads

$$\begin{aligned} \rho_{-11} = & \rho_{-11}^{dc} + \rho_{-11}(\omega_p - \omega_s)e^{-i(\omega_p - \omega_s)t} + \rho_{-11}(\omega_s - \omega_p) \\ & \times e^{-i(\omega_s - \omega_p)t} + \rho_{-11}(2\omega_p - 2\omega_s)e^{-i(2\omega_p - 2\omega_s)t} \\ & + \rho_{-11}(2\omega_s - 2\omega_p)e^{-i(2\omega_s - 2\omega_p)t}. \end{aligned} \quad (16)$$

The system is assumed to satisfy the relation $\rho_{ee} + \rho_{11} + \rho_{00} + \rho_{-1-1} = 1$ and $\rho_{ij}(\omega_k) = \rho_{ji}^*(-\omega_k)$. For example, $\rho_{e1}(\omega_p)$ has the form

$$\begin{aligned} & [i(\omega_p - \omega_{e1}) - \gamma_{e1}]\rho_{e1}(\omega_p) - i[V_p\rho_{-11}^{dc} + V_s\rho_{-11}(\omega_p - \omega_s) \\ & + V_c\rho_{01}(\omega_p - \omega_c) - V_p(\rho_{ee}^{dc} - \rho_{11}^{dc}) - V_s(\rho_{ee}(\omega_p - \omega_s) \\ & - \rho_{11}(\omega_p - \omega_s))] = 0. \end{aligned} \quad (17)$$

In Eq. (17), by exchanging 1 and -1 , $\rho_{e-1}(\omega_p)$ can be obtained. The linear equations of Fourier amplitudes are ready to be solved.

The probe refraction and absorption are proportional to the real and imaginary part of the susceptibility, i.e., $\chi(\omega_p) \propto [\mu_{e1}\rho_{e1}(\omega_p) + \mu_{e-1}\rho_{e-1}(\omega_p)]/(V_p/\gamma)$. Since both transitions $M_{F_g}^g = 1 \leftrightarrow M_{F_g}^g = 0$ and $M_{F_g}^g = -1 \leftrightarrow M_{F_g}^g = 0$ have the same dipole moment, $\chi(\omega_p) \propto [\rho_{e1}(\omega_p) + \rho_{e-1}(\omega_p)]/(V_p/\gamma)$. The pump-probe detuning $\delta = \omega_p - \omega_c$. The dispersion D is proportional to $d\{\text{Re}[\rho_{e1}(\omega_p) + \rho_{e-1}(\omega_p)]/(V_p/\gamma)\}/d(\delta/\gamma)$. Generally, the dispersion of group velocity can be ignored. In the steep dispersion, we have [29]

$$\frac{c}{V_g} = 1 + 2\pi \text{Re} \chi(\omega_p) + 2\pi\omega_p \text{Re} \left(\frac{\partial \chi}{\partial \omega_p} \right). \quad (18)$$

In the real atomic system, $c/V_g = 1 + \Omega D(\delta=0)$, where $\Omega = \pi\omega_p N \mu_{e1}^2 / \gamma^2 \hbar$ [30]. At $\delta=0$, for a positive dispersion, $V_g < c$, which corresponds to a subluminal light propagation, while, for a negative dispersion, $V_g > c$, a superluminal light propagation or even a propagation with negative group velocity.

III. QUANTUM COHERENCE EFFECTS

In order to investigate the effects of saturation field, we first review the quantum coherence effects in a transition $F_e=0 \leftrightarrow F_g=1$ driven by a linearly polarized field and probed by the circular polarized fields [20]. In this case, the system can be seen as a superposition of two Λ -type systems: $M_{F_g}^g = -1 \leftrightarrow F_e=0 \leftrightarrow M_{F_g}^g = 0$ and $M_{F_g}^g = 1 \leftrightarrow F_e=0 \leftrightarrow M_{F_g}^g = 0$, where the state $M_{F_g}^g = 0$ shares the common transition: $F_e = 0 \leftrightarrow M_{F_g}^g = 0$. In a moderate magnetic field, the coherence between the drive Rabi frequency and Zeeman splitting reaches the maximum, leading to the EIA. When the saturation field is added, besides the original two Λ -type systems ($M_{F_g}^g = -1 \leftrightarrow F_e=0 \leftrightarrow M_{F_g}^g = 0$ and $M_{F_g}^g = 1 \leftrightarrow F_e=0 \leftrightarrow M_{F_g}^g = 0$), there are two other Λ -type systems ($M_{F_g}^g = 1 \leftrightarrow F_e=0 \leftrightarrow M_{F_g}^g = -1$, $M_{F_g}^g = -1 \leftrightarrow F_e=0 \leftrightarrow M_{F_g}^g = 1$, and they are identical each other), and two pure two-level systems ($M_{F_g}^g = 1 \leftrightarrow F_e=0$ and $M_{F_g}^g = -1 \leftrightarrow F_e=0$). The main photonic processes include two types of two-photon resonance (which leads to the EIT) [21] and two-photon gain (which leads to the MAS) [9,10]. In the original EIA spectrum [20], with varying the saturation Rabi frequency, the system experiences first two EIT windows and two coherent hole burning, then the coherent hole burning in the EIA peak, and at last several emission peaks. Simultaneously, by the Kramers-Kronig relations, the refraction changes correspondingly. The following Figs. 2, 3, and 5 illustrate the above coherence between the EIA [20] and saturation Rabi frequency.

To model the system shown in Fig. 1, we first define the parameters in the optical Bloch equations, $\Gamma = 1.0$, $\Gamma_0 = 0.01$, $\gamma_{e0} = \gamma_{e1} = (3\Gamma + 2\Gamma_0)/2$ and $\gamma_{10} = \gamma_{01} = 2\Gamma_0$, which are referred to Ref. [28]. We set $\omega_c \approx \omega_{e0}$ and $\omega_s \approx \omega_{e0}$. Here the Zeeman splitting ω_{1-1} between $M_{F_g}^g = 1$ and $M_{F_g}^g = -1$ is set to 5.0, so that $\omega_{10} = \omega_{0-1} = 2.5$. To satisfy that the probe Rabi frequency $2|V_p|$ is much smaller than the drive Rabi frequency $2|V_c|$ and saturation Rabi frequency $2|V_s|$, we always set $|V_p| = 0.01|V_c|$. In the following Figs. 2, 3, and 5, $|V_c| = \omega_{10} = 2.5$, where the EIA happens. For simplicity, we set V_c , V_s and V_p real. We plot the real and imaginary parts of $[\rho_{e1}(\omega_p) + \rho_{e-1}(\omega_p)]/(V_p/\gamma)$, which are used to represent the refraction and absorption.

When the saturation Rabi frequency V_s is small, the two-photon resonance dominates. At $\delta = \pm 2.5$, we observe two main EIT windows due to the two-photon resonance condition of the original drive field and probe field, as shown in Fig. 2. Since V_s is small, the EIA spectrum is preserved [20]. Outside two EIT windows, Autler-Townes peaks at $\delta = \pm 5.0$ are still preserved [31], but where two holes are coherently

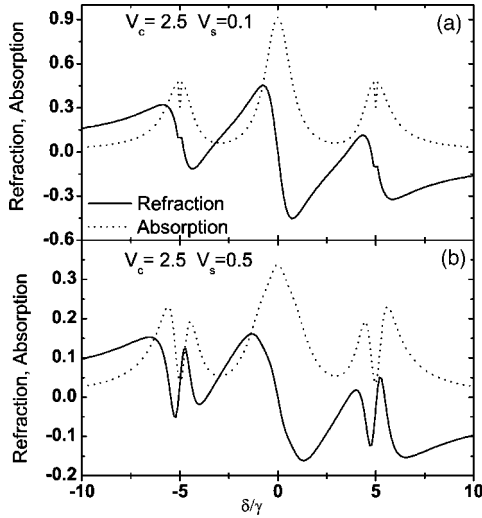


FIG. 2. Absorption and refraction in a small saturation Rabi frequency V_s . (a) $V_c=2.5$, $V_s=0.1$; (b) $V_c=2.5$, $V_s=0.5$. The holes at $\delta=\pm 5.0$ are coherently burned due to the two-photon resonance.

burned, shown in Fig. 2(a). These two holes correspond to the two-photon resonance in the transition $M_{F_g}^g=1 \leftrightarrow F_e=0 \leftrightarrow M_{F_g}^g=-1$ and $M_{F_g}^g=-1 \leftrightarrow F_e=0 \leftrightarrow M_{F_g}^g=1$, where V_s is treated as the pump field. It is also found that the intensity of EIA peak is decreased and the holes are burned deeper when V_s is changed from 0.1 to 0.5, as shown in Fig. 2(a) and Fig. 2(b). At $\delta=\pm 2.5$ and $\delta=\pm 5.0$, the corresponding dispersion is positive.

When the saturation Rabi frequency V_s matches with the drive Rabi frequency V_c , two holes are burned in the original EIA peak [20]. Figure 3 illustrates the evolution of the holes with increasing V_s . The holes in the EIA originates in the

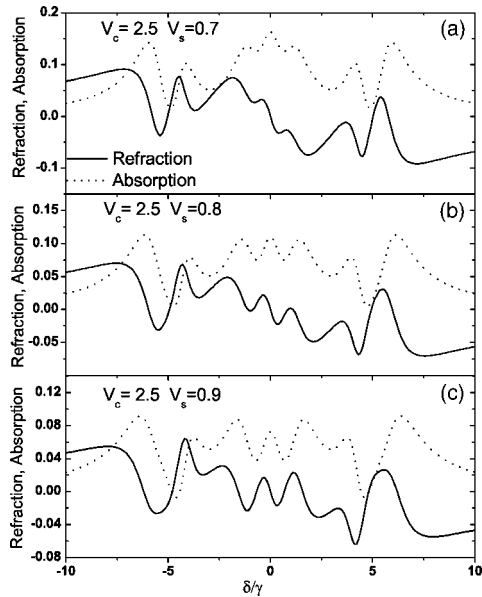


FIG. 3. Absorption and refraction in the moderate saturation Rabi frequency V_s . (a) $V_c=2.5$, $V_s=0.7$; (b) $V_c=2.5$, $V_s=0.8$; (c) $V_c=2.5$, $V_s=0.9$. The holes appearing in the original EIA peak [20] originate in the coherent population oscillations.

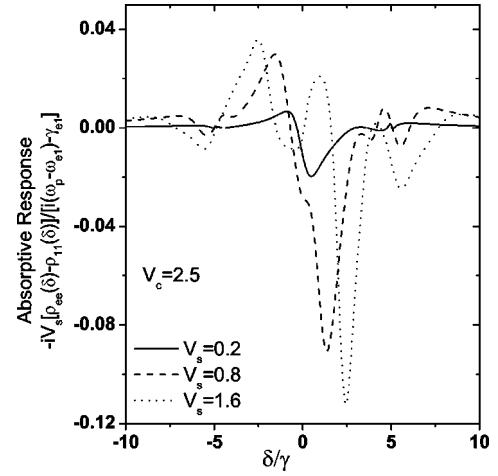


FIG. 4. Absorptive response of the population oscillation (at beat frequency δ) part $iV_s[\rho_{ee}(\delta)-\rho_{11}(\delta)]/[i(\omega_p-\omega_{e1})-\gamma_{e1}]$ in $\rho_{e1}(\omega_p)$. These coherent population oscillations lead to the holes in the EIA peaks [20] in Fig. 3, as well as the gain in the absorption spectrum in Fig. 5.

coherent population oscillations, reported in Refs. [22,23]. The details about this will be explained in the next paragraph. At the same time, increasing the saturation field leads to the decrease of the absorption. However, at $\delta=\pm 2.5$, two EIT windows are very stable due to the two-photon resonance condition. But at $\delta=\pm 5.0$, the transparency points of the original two EIT windows become deeper, until $V_s=0.9$ in Fig. 3(c), and two emission peaks start to appear. In this case, the coupling among the four EIT systems and two pure two-level systems begins to increase, so the multipeak structures appear. In this process, the dispersions also exhibit the complex features. It is noted that, at $\delta=0$, the dispersion is always negative.

Now we consider the influence of the population oscillations $\rho_{ee}(\omega_p-\omega_s)$ and $\rho_{11}(\omega_p-\omega_s)$ on the absorption spectrum. Since $\omega_c \approx \omega_{e0}$ and $\omega_s \approx \omega_{e0}$, in Eq. (17), $\rho_{ee}(\omega_p-\omega_s) - \rho_{11}(\omega_p-\omega_s)$ becomes $\rho_{ee}(\delta) - \rho_{11}(\delta)$. When the drive Rabi frequency $V_c=2.5$, Fig. 4 displays the absorptive response $-iV_s[\rho_{ee}(\delta) - \rho_{11}(\delta)]/[i(\omega_p-\omega_{e1}) - \gamma_{e1}]$ with varying the saturation Rabi frequency V_s . When V_s is small, i.e., $V_s=0.2$, the gain at $\delta=0.2$ is also very small. This gain induces only a small decrease in the original EIA peak [20], as shown in Fig. 2. When V_s is moderate, say, $V_s=0.8$, there is a large gain in the absorption spectrum. Hence, the coherent population oscillations $[\rho_{ee}(\delta) - \rho_{11}(\delta)]$ with a beat frequency δ cause the holes in the original EIA peak [20]. However, when $V_s=1.6$, the large gain is obtained at $\delta=2.5$. Combined with the EIT effect, in the following Fig. 5, emission peaks are observed.

When we continue to increase the saturation Rabi frequency V_s , Mollow absorption effects play an important role and several emission peaks appear in the absorption spectrum. When $V_s=1.4$, as shown in Fig. 5(a), the absorption at $\delta=0$ starts to disappear, where the transition from absorption to emission takes place [32,33]. We also observe four emission peaks in this figure. When $V_s=2.5$ in Fig. 5(b), the gain appears in a wide spectral region. At $\delta=\pm 2.5$, there exist two

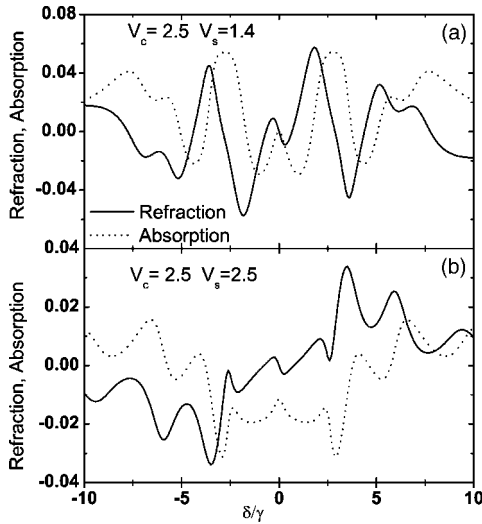


FIG. 5. Absorption and refraction in large saturation Rabi frequency V_s . (a) $V_c=2.5$, $V_s=1.4$; (b) $V_c=2.5$, $V_s=2.5$. Mollow absorption effects play more and several emission peaks appear.

large emission peaks. These two emission peaks come from a combination of Mollow absorption effects [9,10] and coherent population oscillations [22,23], shown as the dotted line in Fig. 4. At $\delta=0$, the negative dispersion with gain is obtained. Hence, when $V_s \geq 1.4$, the zero pump-probe detuning should be a suitable point to perform the experiment of superluminal light propagation.

In the above Figs. 2, 3, and 5, the refractions also exhibit very fruitful features with varying the saturation Rabi frequency V_s . It is noted that, for any values of V_s , the dispersion at $\delta=0$ is kept to be negative, but its absolute value of dispersion is decreasing. Furthermore, in the region of gain, not only the negative dispersion, but also the positive dispersion are obtained, as shown in Fig. 5. These results come from the coherence among the drive Rabi frequency, saturation Rabi frequency, and the Zeeman splitting.

We also investigate the quantum coherence effects of the saturation field when the drive Rabi frequency V_c is very small or very large. When $V_c=0.5$, the system first experiences four EIT windows, then MAS with varying the saturation Rabi frequency V_s from 0.2 in Fig. 6(a), via 1.0 in Fig. 6(b), to 2.0 in Fig. 6(c) [32,33]. In contrast, when $V_c=5.0$, the spectra of absorption and refraction are very stable for a small saturation Rabi frequency $V_s=1.0$, as shown in Fig. 7(a). While, for a large $V_s=5.5$, two outside EIT windows move from the pump-detuning center and the middle EIT window becomes very wide, as shown in Fig. 7(b). In the second case, instead of the MAS in two pure two-level systems, two-photon resonance in four Λ -type systems dominates the main coherence effects of the transition $F_e=0 \leftrightarrow F_g=1$.

In the theoretical treatment, besides the single-photon process and two-photon process, three-photon process is also included, such as the terms of Fourier amplitude: $\rho_{e0}(\omega_c + \omega_p - \omega_s)$, $\rho_{e0}(\omega_c - \omega_p + \omega_s)$, and $\rho_{ei}(2\omega_s - \omega_p)$, etc. The quantum profile of four-wave mixing (FWM) will be the same order as the $\rho_{ei}(\omega_p)$ [34]. By varying the drive Rabi frequency V_c or saturation Rabi frequency V_s , the maximum

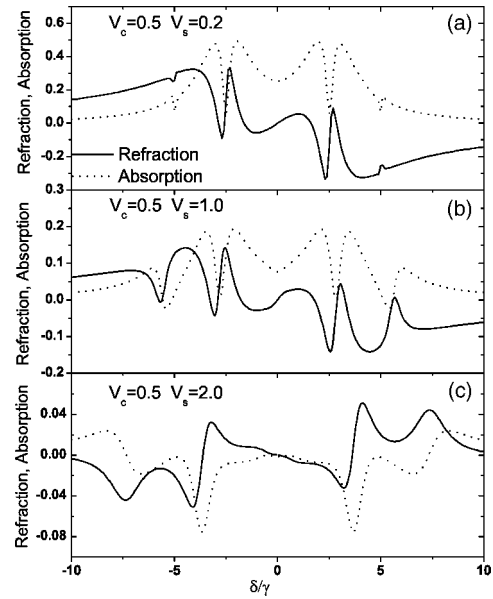


FIG. 6. Absorption and refraction in a small drive Rabi frequency V_c . (a) $V_c=0.5$, $V_s=0.2$; (b) $V_c=0.5$, $V_s=1.0$; (c) $V_c=0.5$, $V_s=2.0$. The system experiences four EIT windows and MAS with varying V_s .

quantum profiles of the FWM will be found. Further discussion about this will appear in another publication.

IV. SUMMARY

In this paper, we have investigated the quantum coherence effects for a transition $F_e=0 \leftrightarrow F_g=1$. When the atom is driven by a linearly polarized field, probed by the circularly

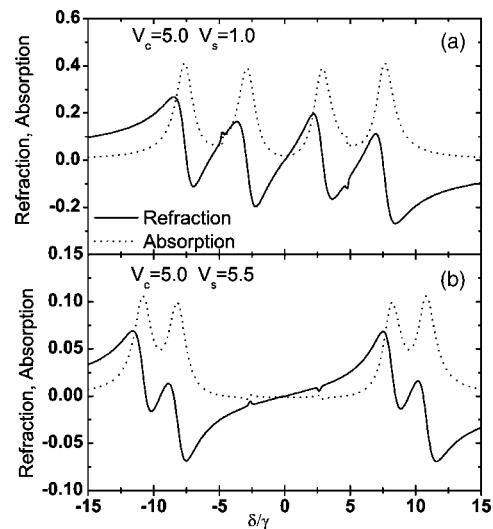


FIG. 7. Absorption and refraction in large drive Rabi frequency V_c . (a) $V_c=5.0$, $V_s=1.0$; (b) $V_c=5.0$, $V_s=5.5$. EIT windows are preserved, but moving away from the detuning center.

polarized fields, without the saturation field, EIA with negative dispersion is obtained in the moderate drive Rabi frequency and magnetic field [20]. Then the drive Rabi frequency is fixed at the point of EIA occurring. For a small saturation Rabi frequency, the holes in the Autler-Townes peaks outside the two EIT windows are burned due to the two-photon resonance. When the saturation Rabi frequency matches with the drive Rabi frequency, the hole burning in the EIA spectrum is found due to the coherent population oscillations. When the saturation Rabi frequency is large enough, several emission peaks are observed due to the Mollow absorption effects. With the increment of the saturation Rabi frequency, the dispersion at the pump-probe detuning center is kept negative, which predicts the superluminal light propagation. Finally, in the saturation field, the quantum co-

herence effects for a very small or large drive Rabi frequency are also discussed.

ACKNOWLEDGMENTS

The work was supported by National Natural Science Foundation of China under Grant Nos. 10334010, 10304001, 10328407, and 90101027. The work was also supported by the special fund from Ministry of Science and Technology of China, the National Key Basic Research Special Foundation under Grant No. TG1999075207. The project was partly sponsored by the Scientific Research Foundation for the Returned Overseas Chinese Scholars, State Education Ministry. We thank Professor Z. J. Xia and Professor H. B. Jiang for stimulating and helpful discussions.

-
- [1] S. E. Harris, *Phys. Today* **50** (7), 36 (1997).
 [2] E. Arimondo, in *Progress in Optics*, edited by E. Wolf (Elsevier Science, Amsterdam, 1996), Vol. 35, p. 257.
 [3] M. D. Lukin *et al.*, *Laser Phys.* **9**, 759 (1999).
 [4] A. Lezama, S. Barreiro, and A. M. Akulshin, *Phys. Rev. A* **59**, 4732 (1999).
 [5] A. M. Akulshin, S. Barreiro, and A. Lezama, *Phys. Rev. A* **57**, 2996 (1998).
 [6] A. M. Akulshin, S. Barreiro, and A. Lezama, *Phys. Rev. Lett.* **83**, 4277 (1999).
 [7] C. Andreeva, S. Cartaleva, Y. Dancheva, V. Biancalana, A. Burchianti, C. Marinelli, E. Mariotti, L. Moi, and K. Nasyrov, *Phys. Rev. A* **66**, 012502 (2002).
 [8] A. Lipsich, S. Barreiro, A. M. Akulshin, and A. Lezama, *Phys. Rev. A* **61**, 053803 (2000).
 [9] B. R. Mollow, *Phys. Rev. A* **5**, 2217 (1972).
 [10] F. Y. Wu, S. Ezekiel, M. Ducloy, and B. R. Mollow, *Phys. Rev. Lett.* **38**, 1077 (1977).
 [11] W. R. Bennett, Jr., *Phys. Rev.* **126**, 580 (1962).
 [12] W. E. Lamb, Jr., *Phys. Rev.* **134**, A1429 (1964).
 [13] M. Sargent III, *Phys. Rep.*, *Phys. Lett.* **43**, 223 (1978).
 [14] Z. H. Xiao, J. H. Wu, H. F. Zhang, and J. Y. Gao, *Phys. Lett. A* **310**, 363 (2003).
 [15] P. R. Berman, *Adv. At. Mol. Phys.* **13**, 55 (1977).
 [16] A. A. Gorokhovskii, R. K. Kaarli, and L. A. Rebane, *JETP Lett.* **20**, 216 (1974).
 [17] W. E. Moerner, *Persistent Spectral Hole Burning: Science and Application* (Springer, Berlin, 1988).
 [18] Matthew S. Bigelow, Nick N. Lepeshkin, and Robert W. Boyd, *Phys. Rev. Lett.* **90**, 113903 (2003).
 [19] Matthew S. Bigelow, Nick N. Lepeshkin, and Robert W. Boyd, *Science* **31**, 200 (2003).
 [20] Y. Gu, Q. Sun, and Q. Gong, *Phys. Rev. A* **67**, 063809 (2003).
 [21] A. F. Huss, E. A. Korsunsky, and L. Windholz, *J. Mod. Opt.* **49**, 141 (2002).
 [22] R. W. Boyd *et al.*, *Phys. Rev. A* **24**, 411 (1981).
 [23] L. W. Hillman, R. W. Boyd, J. Krasinski, and C. R. Stroud, Jr., *Opt. Commun.* **45**, 416 (1983).
 [24] L. M. Barkov *et al.*, *Opt. Commun.* **70**, 467 (1989).
 [25] S. A. Diddams, J. C. Diels, and B. Atherton, *Phys. Rev. A* **58**, 2252 (1998).
 [26] K. Bergmann, H. Theuer, and B. W. Shore, *Rev. Mod. Phys.* **70**, 1003 (1998).
 [27] P. Cerez and F. Hartmann, *IEEE J. Quantum Electron.* **QE13**, 344 (1977).
 [28] A. D. Wilson-Gordon, *Phys. Rev. A* **48**, 4639 (1993).
 [29] S. E. Harris *et al.*, *Phys. Rev. A* **46**, R29 (1992).
 [30] D. Bortman-Arbiv, A. D. Wilson-Gordon, and H. Friedmann, *Phys. Rev. A* **63**, 043818 (2001).
 [31] E. Paspalakis and P. L. Knight, *Phys. Rev. A* **66**, 015802 (2002).
 [32] A. D. Wilson-Gordon and H. Friedmann, *J. Mod. Opt.* **49**, 125 (2002).
 [33] S. Menon and G. S. Agarwal, *Phys. Rev. A* **59**, 740 (1999).
 [34] M. D. Lukin, P. R. Hemmer, and M. O. Scully, *Adv. At., Mol., Opt. Phys.* **42**, 347 (2000).